JOURNAL OF PROPULSION AND POWER
Vol. 14, No. 2, March–April 1998

Spray Structures of Liquid Jets Atomized in Subsonic Crossflows

Pei-Kuan Wu,* Kevin A. Kirkendall,† and Raymond P. Fuller‡
Taitech, Inc., Dayton, Ohio 45440
and
Abdollah S. Nejad§
U.S. Air Force Research Laboratory, Wright–Patterson Air Force Base, Ohio 45433

The structures of spray plumes from 0.5-mm waterjets injected into a subsonic crossflow were experimentally investigated using phase Doppler particle anemometry. Droplet size, axial velocity, and volume flux were measured across the spray plume at several axial distances downstream of the injector exit. Results indicate that large droplets can be found in the central portion of the spray plume for cases with small liquid/air momentum flux ratios and in which the momentum exchange between column waves and the airstream is significant. For cases with large-momentum flux ratios, the droplet size distribution exhibits a concave-layered structure, with the peak on the centerline and large droplets at the top. Droplets were found to concentrate in a small area within the spray plume, which indicates that the liquid mass distribution is not uniform. The height of the maximum volume flux locations, an indicator of the location of the highest concentration of droplets, was measured and correlated with momentum flux ratios and axial distances. It was found that more droplets are distributed toward the upper portion of the spray plume for larger momentum flux ratios. Spray penetration, spray width, penetration-to-width ratio, and spray cross-sectional area were also found to increase with the momentum flux ratio.

Nomenclature

A = cross-sectional area
d = injector diameter
Oh_d = Ohnesorge number, $\mu_f/(\rho_f d\sigma)^{1/2}$
$\bar{q}$ = liquid/air momentum flux ratio, $\rho_f v_j^2/\rho_\infty u_\infty^2$
Re_{fd} = Reynolds number, $\rho_f d v_j/\mu_f$
Re_{gd} = Reynolds number, $\rho_\infty d u_\infty/\mu_\infty$
SMD = Sauter mean diameter, $\sum d_i^3/\sum d_i^2$, i for all droplets
u = velocity component in the x direction
v = velocity component in the y direction
We_{fd} = Weber number, $\rho_f d v_j^2/\sigma$
We_{gd} = Weber number, $\rho_\infty d u_\infty^2/\sigma$
x = distance in the airstream direction
y = distance in the direction of liquid injection
y_m = height of the maximum volume flux location
y_t = height of the top of spray plume
z_w = spray width
μ = molecular viscosity
ρ = density
σ = surface tension

Subscripts
f = liquid-phase property
j = liquid property at injector exit
p = property of droplets
∞ = air property in the freestream
% = percentage of injected liquid mass contained in the specified area

Superscript
$-$ = flux-averaged property across the spray plume

Introduction

IMPROVEMENTS in combustion efficiency and reductions in pollutant emissions in propulsion systems will require improved technology for the distribution of specific quantities of atomized fuel to specific locations. Therefore, liquid-fuel jet-breakup processes, droplet transport dynamics, and spray structures must be investigated and understood. Numerous studies have been performed to characterize these processes for liquid-fuel jets injected perpendicularly into an airstream.[1–20] Because of the complexity of these processes, however, both the current understanding of fundamental atomization physics and the existing database of spray structures are still very limited. The present study focuses on the characterization of downstream spray structures in an effort to relate the structures to jet operating conditions and to provide correlations and a database for improvements in atomization control technology. Because spray structures are closely related to column breakup processes, a brief review of the literature on the entire spray will be presented.

For liquid-fuel injection into an air crossflow it is well known that the spray field can be divided into three regimes: 1) column, 2) ligament, and 3) droplet regimes. Column trajectories determine the location of droplet formation.[1–5] Wu et al.[1] analyzed column trajectories by balancing the liquid acceleration in the axial direction with aerodynamic forces. A parabolic correlation was obtained and found to agree with experimental results. The cross-fracture locations were also predicted by employing the time scale of the secondary breakup of a spherical droplet.[1] The drag coefficient, however, was found to vary when the correlation was tested with trajectories reported in other studies, indicating that the trajectory

Received April 11, 1997; revision received Sept. 29, 1997; accepted for publication Oct. 8, 1997.

*Senior Research Scientist, 3675 Harmeling Drive; currently Senior Principal Engineer, Kaiser Marquardt, 16555 Saticoy Street, Van Nuys, CA 91406. E-mail: wu@marquardt.com. Member AIAA.
†Research Engineer, 3675 Harmeling Drive.
‡Research Scientist, 3675 Harmeling Drive. Member AIAA.
§Senior Research Scientist, Aero Propulsion and Power Directorate; currently Director of Engineering, Kaiser Marquardt, 16555 Saticoy Street, Van Nuys, CA 91406.

might be affected by the air boundary-layer thickness and the liquid-injection flow profile.[2] Oda et al.[3,4] used laser tomography to measure the column thickness at various heights after the column was deformed. The liquid column was treated as a liquid sheet and a Kelvin–Helmholtz instability model was applied to determine the cross-fracture location. Inamura et al.[5,6] investigated column trajectories of water and slurry jets and found that the x/d of the cross-fracture point was fairly constant over a wide range of jet operating conditions. This phenomenon was later verified by Wu et al.[1] over a wider range of jet operating conditions and was explained using a phenomenological theory. Nguyen and Karagozian[7] used an analytical/numerical model to simulate the interaction of the airstream and liquid column. Trajectories were computed for liquid jets under both reacting and nonreacting conditions. Fuller et al.[8] extended the momentum analysis developed in Wu et al.[1] to include the effect of injection angle on column trajectories and breakup processes. Injection angles of 30, 45, 60, 75, and 90 deg were considered and good agreement was obtained between the measured trajectories and the predicted values.

While the trajectory determines the location of droplet formation, the mechanisms of droplet formation depend on column wave growth. Schetz et al.[9] distinguished waves as leeward and windward and related the windward waves to the liquid acceleration caused by aerodynamic drag forces in a supersonic airstream. Ingebo[10] described the waves as capillary and acceleration waves, and atomization was depicted as a process of forming ligaments from the crests of column waves. Wu et al.[1] observed that the column exhibits surface breakup (as distinct from column breakup) as droplets are stripped away from the column periphery, even when the windward surface is smooth. The effects of liquid properties on the wave growth process and the resulting spray field in supersonic crossflows were discussed by Nejad and Schetz.[11,12]

Spray structures in the droplet regime have generally been discussed in terms of spray penetration,[13–16] spray width,[3,5,6,17] and droplet size.[18–20] Schetz and Padhye[13] performed a momentum analysis on maximum penetration heights and found that the maximum penetration height is the distance required to redirect the liquid jet injection momentum flux to the airstream direction. The penetration height was measured at 6.25 jet diameters downstream and was correlated with $\bar{q}$. Chen et al.[14] used a Mie scattering technique to investigate jet trajectories from the nozzle exit to about 60 nozzle diameters downstream and developed a three-parameter exponential function to account for the three spray regimes. Wu et al.[2] applied the momentum equations of a spherical droplet to characterize the spray trajectory in the droplet regime, where droplets are spherical. Correlations for spatial locations, droplet velocities, and droplet sizes along the top boundary of the spray plume were obtained. A power-law empirical correlation of the trajectory was also obtained for conditions under which droplet velocity data are not required. Functions with different forms have been used by other researchers.[13,14]

Spray widths have been investigated by Inamura et al.[5,6] and Oda et al.[17] Inamura et al. employed a photographic method and recorded images from the top of the spray field. A correlation of spray widths was found to be a function of $\bar{q}$ and x/d. Oda et al. proposed a half spray width defined on the plane of the maximum local mass flux. The width was used to correlate the mass flux spatial distribution across the spray plume based on measured mass fluxes on the centerline.

Droplet sizes in the droplet regime were measured by Ingebo[10] using a scanning radiometer. A correlation of spray mean diameters was obtained as a function of the product of Weber and Reynolds numbers and a pressure-sensitive dimensionless term. Schetz and Padhye[13] employed a microscopic photography method to measure droplet sizes for injectors of various geometries. The injector geometry was found to have significant effects on the average droplet size. Less and Schetz[18] applied a high-sampling-rate Fraunhofer diffraction system to investigate the temporal variation of droplet size in a supersonic crossflow. The variation was related to the unsteadiness of the jet breakup processes. A planar liquid laser-induced fluorescence (PLIF) technique was employed by Seay et al.[19] to determine the spread, penetration, and structure of the spray plume generated from a radial airblast injector in a subsonic crossflow. Results agreed with those obtained by phase Doppler particle anemometry (PDPA). A spatial unmixedness parameter was used to characterize the degree of fuel/air mixing. Kihm et al.[20] measured droplet size using a laser diffraction method, and an empirical correlation was developed to predict droplet size at various locations. Inamura et al.[6] used PDPA to measure droplet size in the spray plume and found that droplet size peaks at the same location as the liquid mass flux. Most recently, Inamura and Nagai[21] used an isokinetic sampling probe and PDPA to characterize the spray structures of 1- and 2-mm waterjets in a subsonic airstream. Mass flux distributions were found to follow normal distribution functions. Droplet sizes and velocities were measured at various axial locations.

The objectives of the present study were to characterize spray structures in terms of droplet size, velocity, and volume flux; to relate spray structures to column breakup processes; and to develop correlations for the prediction of spray structures. The study focused on the spray structures of 0.5-mm waterjets in a subsonic airstream; $\bar{q}$ was varied from 5.3 to 59.1. Two-dimensional spray structures were emphasized and several different spray phenomena were identified. These results were compared with those obtained by Inamura and Nagai[21] for 1- and 2-mm waterjets with $\bar{q}$ from 6 to 12. This paper begins with a description of the apparatus and instrumentation, followed by a discussion of the test conditions. The results are then discussed, treating cross-sectional distributions, centerline properties, flux-averaged properties, and spray correlations. This paper concludes with a summary of the present findings on the spray structures of liquid jets in a subsonic crossflow.

Experimental Methods

Apparatus and Instrumentation

Liquid jets were injected vertically upward into a subsonic wind tunnel with the nozzle exit flush with the tunnel bottom wall. Detailed descriptions of the design and operation of the tunnel can be found elsewhere.[22,23] The wind tunnel has a rectangular test section with a width of 125 mm, a height of 75 mm, and a length of 406 mm. Quartz windows on the top and both sides of the test section provide access for laser diagnostics and flow visualization. Vacuum pumps at the end of the tunnel maintain a constant back pressure at 20 kPa. A continuous airflow is provided by two large reciprocating compressors that produce a total mass flow rate of up to 2.2 kg/s at 5.1 MPa. The air Mach number is controlled by adjusting a variable-area nozzle device downstream of the test section to obtain the correct area ratios between the choked point and the test section.[22,23] Air pressures and temperatures are measured using strain gauges and k-type thermocouples and monitored by a personal computer. The uncertainties of the pressure and temperature measurements are less than 1%. Air velocities are measured using laser Doppler velocimetry. Air mean velocities exhibit a standard deviation of 2% across the entire tunnel, and axial turbulence intensities are less than 3% at the center of the tunnel. The air boundary-layer thickness was measured to be less than 4 mm at the injection location.

The liquid injection system consists of a large injection tank, a Coriolis-type flow meter, and an injector unit. The injection tank has an internal volume of 0.144 m^3 and is rated for 3 MPa. Before the experiment, test liquids are filled into the injection tank and pressurized with high-pressure nitrogen. Liquid mass flow rates are controlled by adjusting the nitrogen

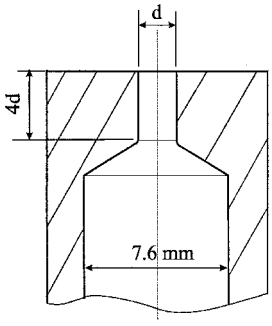

Fig. 1 Injector geometry.

pressure and are measured using a Coriolis-type flow meter. The flow meter is calibrated to an uncertainty of less than 1%. Measured liquid mass flow rates are used to calculate v_j based on the measured liquid density and the injector exit diameter. A sketch of the injector geometry is shown in Fig. 1. The injector passage has an inlet diameter of 7.6 mm, followed by a 60-deg taper to an injector exit diameter of 0.5 mm, followed by a straight section with a length/diameter ratio of 4. The transition from the tapered section to the straight injector exit section was rounded to avoid cavitation. The injector passage was designed to produce very low liquid turbulence intensity at the exit, so that the effects of air crossflows could be studied without the presence of extraneous mechanisms.

Droplet properties within the spray plume were measured using a single-component Aerometric PDPA with a 10-mW helium–neon laser and a counterbased processor. The focal lengths of the collimating and transmitting lenses were 160 and 495 mm, respectively. The receiver aperture was 150 mm in diameter. The collected light was passed through a 100-μm slit to reduce the probe volume. Light was collected at 150 deg from the transmitter (refractive scattering). The PDPA was calibrated with an object of 200 μm before experimentation. The measurement was within 2% of the object size and indicated that the detector spacing and the receiver optics of the PDPA were adequate.[24] More detailed information about the operation and the performance of PDPA can be found in McDonell and Samuelsen.[24]

Droplet size, axial velocity, and volume flux were measured at increments of 2.54 mm in the transverse and spanwise directions across the spray plume. Measurements were ceased when the measured volume flux fell below about 0.02 cc/s/cm^2. This approach yields an uncertainty of $\pm 2.5d$ for the measurements of y_t/d, y_m/d, and z_w/d. Droplet properties were averaged over more than 1500 droplets at each location. The total liquid flow rate was calculated by integrating the measured volume flux across the entire spray plume. The mean and standard deviation of the ratio of measured- to injected-liquid flow rates were 1.80 and 46%, respectively. The ratio of 1.80 is attributed to the large droplet number density in the spray core region and the inaccuracy of the probe volume determination.[24] Therefore, the volume flux results shown in the present study are used to establish trends and order of magnitude comparisons only. Measurements were performed at x/d = 200, 300, and 500 to avoid problems of nonspherical ligaments and high droplet number densities. Validation rates of the PDPA measurements were generally above 90%. The validation rate, however, fell to about 60% in some spots near the lower portion of the plume for the two largest v_j conditions.

Test Conditions

Water was used as the test liquid, and its properties were measured before experimentation. Liquid density was measured using hydrometers that are accurate to 0.5 kg/m^3. A Cannon/Fenske viscometer was used to measure liquid viscosity with a measurement uncertainty of less than 0.2%. Liquid surface tension in air was measured using a ring tensiometer that is accurate to 0.0005 N/m. Measured liquid properties were as follows: liquid density was 998 kg/m^3, liquid viscosity was 9.56×10^{-4} kg/m/s, and surface tension was 0.0705 N/m. The injector exit diameter was 0.5 mm, and the injection velocity was varied from 12.8 to 42.5 m/s. The air Mach numbers were limited to 0.2, 0.3, and 0.4, and the air density was calculated to be 1.633 kg/m^3. Measurements were performed at x/d of 200, 300, and 500. These test conditions yield jet dynamic parameters as follows: $\bar{q}$ of 5.3–59.1, We_{gd} of 54–217, We_{fd} of 1152–12,800, Re_{gd} of 3.12×10^3–1.28×10^4, Re_{fd} of 6.66×10^3–2.22×10^4, and Oh_d of 5.1×10^{-3}.

Results and Discussion

Results of the study of spray structures will be discussed in terms of cross-sectional distributions, centerline properties, flux-averaged properties, and spray correlations. This discussion emphasizes the characterization of spray structures and their relationship to the jet breakup processes. Correlations of spray properties are constructed for the prediction of spray structures and the development of better atomization control technology.

Cross-Sectional Distributions

Cross-sectional distributions of SMD, u_p, and volume flux were acquired using a PDPA. Figure 2 shows the cross-sectional distributions generated by a waterjet injected at a velocity of 12.8 m/s into a Mach 0.3 airflow with $\bar{q}$ = 9.5. In Fig. 2a, the SMD varies from 67 to 109 μm. The largest SMD nearly agrees with the prediction of 103 μm from Wu et al.[2]

The cross-sectional distribution exhibits a region of relatively large droplets in the center area of the spray plume. From the bottom wall up, the SMD first increases to a large value and then decreases before again increasing. The region of large droplets is located in the same area as the spray core, identified as the region of maximum volume flux in Fig. 2c. Nejad and Schetz[11] and Inamura and Nagai[21] also observed that the maximum SMD appears in the spray core. They found that the centerline droplet size distribution near the injector exhibits a maximum SMD in the spray core, regardless of the injection conditions. As the axial distance increases, the larger droplets in the spray core penetrate into the airstream and cause the SMD to peak at the top of the spray plume for cases of small u_∞.[21] For cases of large u_∞, however, the larger droplets remain in the central portion of the spray plume.[21] The distribution shown in Fig. 2a agrees with the results of Inamura and Nagai[21] for large u_∞, and indicates that the larger droplets remain in the spray core, even at x/d = 300. This phenomenon is related to the momentum exchange between column waves and the airstream and will be discussed in relation to Fig. 3a. Some larger droplets still penetrate to the top and the periphery of the spray plume, which results in a concave-layered structure outside the spray core.

Droplet axial velocities for the same spray are shown in Fig. 2b. Droplet velocity was varied from 63 to 84 m/s, with u_∞ = 103 m/s. A lower-velocity region can be identified in the center and lower portion of the spray plume. This is a wake region caused by the presence of the liquid column near the injector exit. Two higher-velocity regions were observed on each side of the wake region, which was attributed to the higher air velocity around the liquid column near the injector exit and before significant column deformation. Column deformation causes significant momentum exchange and slows down the airstream near the upper portion of the spray plume. The high-velocity region persists to downstream locations and thus appears as lobes in the contour plot. A lower-velocity region was found near the top because of the large momentum exchange caused by the column deformation.

The volume flux distribution is shown in Fig. 2c with a maximum value of 5.5 cc/s/cm^2. Volume flux gradually decreases from the center to the edge of the plume. The region of large volume flux indicates an area of high droplet concen-

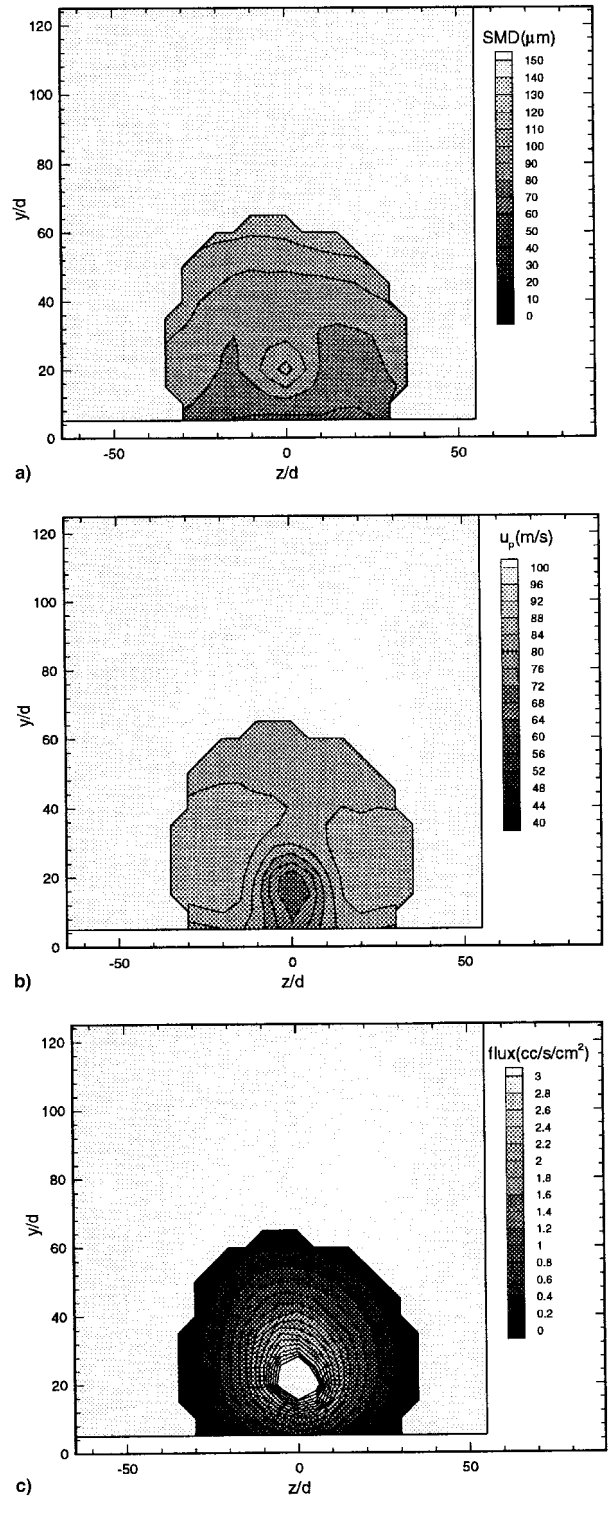

Fig. 2 Cross-sectional distributions of a) SMD, b) u_p, and c) volume flux of waterjets injected into a Mach 0.3 crossflow at x/d = 300, v_j = 12.8 m/s, and $\bar{q}$ = 9.5.

tration and contains a significant amount of the injected liquid. According to the measurements to be discussed, 30 and 70% of the injected liquid are concentrated in areas of about 7 and 25% of the spray plume, respectively. The spatial distribution of liquid droplets is apparently not uniform. Inamura and Nagai[21] and Oda et al.[17] suggest that the distribution of mass flux follows a normal distribution function. Present results agree qualitatively with their findings.

Results for a waterjet injected into a Mach 0.3 airflow at an injection velocity of 19.0 m/s are shown in Fig. 3. Measurements were made at x/d = 300 with $\bar{q}$ = 21.7. The SMD was found to vary from 38 to 106 μm, with small droplets near the bottom wall and large droplets at the top (Fig. 3a). The largest SMD is nearly the same as in the previous case (v_j = 12.8 m/s). The smallest SMD, however, is significantly smaller than in the previous case. In the previous case, droplet impingement on the bottom wall was observed; this process causes the SMD to increase and, therefore, also increases the smallest SMD. The SMD distribution exhibits a concave-layered structure with the peak on the centerline. In this case droplets maintain most of their transverse momentum and reach the top of the plume. On the other hand, droplets also penetrate into the airstream in the spanwise direction, and larger droplets are also found at the outer edge of the plume, because of their large momentum. Therefore, the distribution exhibits a concave-layered structure as depicted in Fig. 3a. For these conditions, the distribution is not highly three dimensional, and a line-of-sight measurement, such as the laser diffraction technique, may provide a satisfactory analysis of droplet size distributions.

Figures 2a and 3a indicate that the appearance of large SMD in the spray core depends not only u_∞, as suggested by Inamura and Nagai,[21] but also on v_j. These observations are related to the momentum exchange between the column waves and the airstream, which depends on column curvature and breakup mode. As discussed in Wu et al.,[1] the liquid column follows the trajectory of a parabolic function. Because the column always breaks at the same axial location, it experiences much sharper curvature toward the downstream direction for smaller $\bar{q}$ conditions. In these cases, the column is almost parallel to the airstream direction. The interaction between the column waves and the airstream is intense and their momentum exchange is significant. Droplets generated from these waves, therefore, do not have large transverse momentum and cannot penetrate very far into the airstream (Fig. 2a). This argument is also supported by the fact that a significant wake region is always observed in these cases. For large $\bar{q}$ conditions, the column curvature is not sharp and the momentum exchange is not intense. Droplets thus retain large transverse momentum and penetrate farther into the airstream (Fig. 3a).

Inamura and Nagai[21] observed a shift in the maximum SMD location from the top of the spray plume to the spray core when u_∞ was increased and $\bar{q}$ was kept constant. A possible explanation is the transition of column breakup modes and the resulting liquid/air momentum exchange. It is to be expected that the momentum exchange will be more intense for conditions of larger d and u_∞, depending on the extent of the wake region as determined based on the droplet velocity measurements of the present study and those of Inamura and Nagai. Therefore, the SMD peaks in the spray core when d and u_∞ increase. The effects of breakup mode on the momentum exchange, however, have not been quantified; further studies of the column breakup process are required to resolve this issue.

Figure 3b shows the droplet axial velocity distribution u_p for the same spray. The droplet velocity varies from 78 to 92 m/s. These velocities are generally larger than those in the previous case, indicating a smaller deceleration of the airstream. As a result, a less significant wake region can be observed, and two large-velocity regions appear around the wake region.

The measured volume flux distribution, shown in Fig. 3c, exhibits a structure similar to that in Fig. 2c, although the large flux region is located further away from the bottom wall in this case. The smaller wake region and higher maximum flux location are attributed to the smaller curvature of the liquid column for larger $\bar{q}$ conditions, as discussed earlier. The maximum volume flux is 2.5 cc/s/cm^2, indicating that the spray is spatially less concentrated than in the previous case. This phenomenon is consistent with the observation of Inamura and

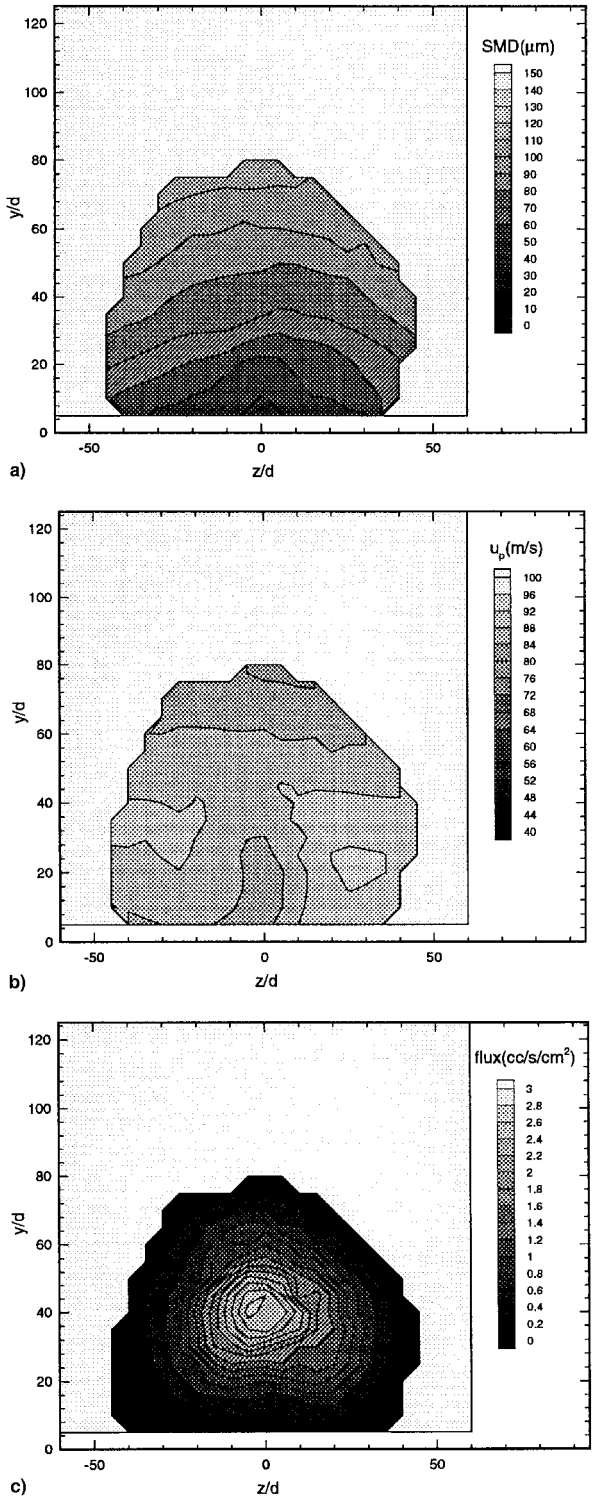

Fig. 3 Cross-sectional distributions of a) SMD, b) u_p, and c) volume flux of waterjets injected into a Mach 0.3 crossflow at x/d = 300, v_j = 19.0 m/s, and $\bar{q}$ = 21.7.

Nagai for 1- and 2-mm waterjets: the maximum volume flux decreases as $\bar{q}$ increases.

Figure 4 shows the cross-sectional distribution for a waterjet injected into a Mach 0.4 airstream at v_j = 19.3 m/s and $\bar{q}$ = 12.2. As for the previous cases, the SMD distribution exhibits an area of large droplets near the center of the spray plume, although the variation in SMD is smaller (from 46 to 72 μm). The reduction in maximum SMD, as compared to the previous cases, is caused by the increase in air velocity from 103 to 137 m/s. The minimum SMD does not vary significantly when compared to that shown in Fig. 3a, although the area containing smaller droplets increases. These results suggest that the SMD variation within the spray plume decreases as u_∞ increases because of the decrease in the maximum SMD. Distributions of droplet axial velocity and volume flux are shown in Figs. 4b and 4c, respectively. Droplet axial velocity varies from 103 to 126 m/s, while the maximum volume flux is 2.7 cc/s/cm^2. It is apparent that these structures are three dimensional and depend heavily on the near-field breakup processes of the liquid column.

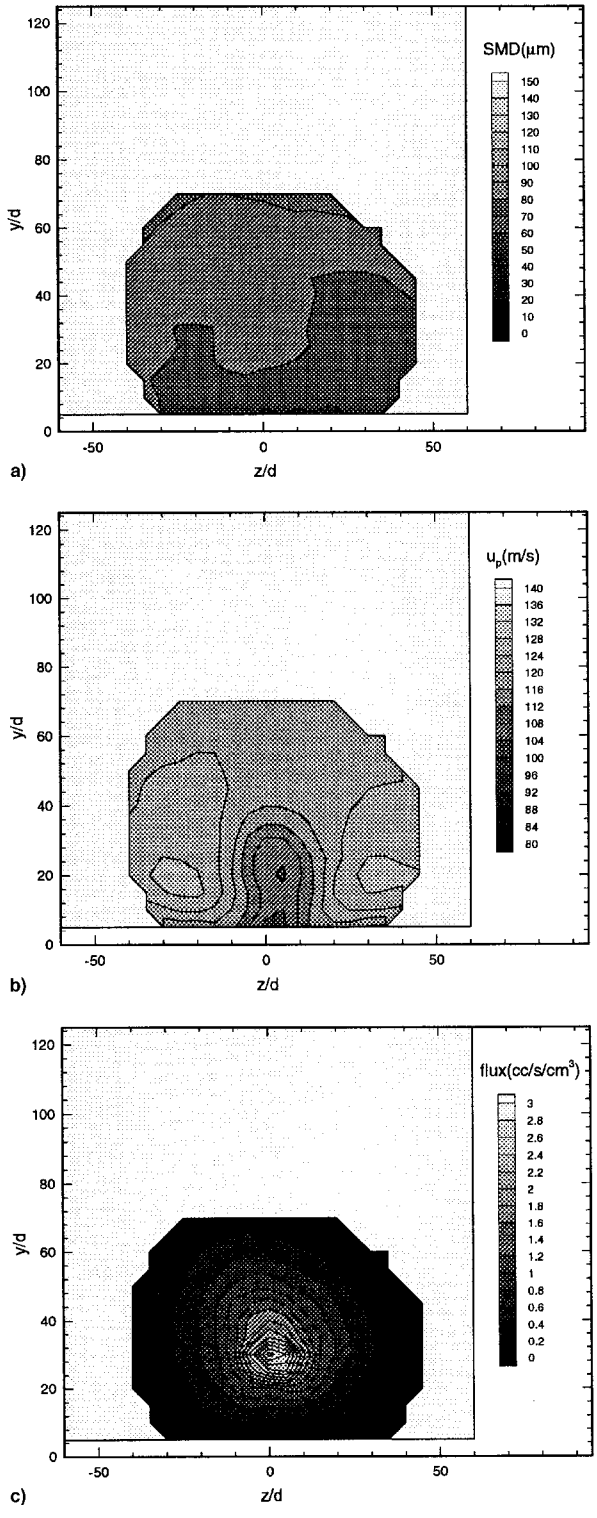

Fig. 4 Cross-sectional distributions of a) SMD, b) u_p, and c) volume flux of waterjets injected into a Mach 0.4 crossflow at x/d = 500, v_j = 19.3 m/s, and $\bar{q}$ = 12.2.

Centerline Properties

Centerline properties of the spray plume for a waterjet injected into a Mach 0.3 air crossflow at injection velocities of 12.8, 19.3, and 29.0 m/s are plotted in Fig. 5 as functions of y/d. The location of the maximum flux shifts upward and the value decreases as v_j increases. At v_j = 12.8 m/s, u_p shows a region of smaller values at y/d around 20. This region is a wake region caused by the presence of the liquid column and the momentum exchange between the column wave and the airstream. As v_j increases, u_p exhibits a smoother curve and increases in overall magnitude. The wake region can be used as an indicator of the extent of the momentum exchange between the column waves and the airstream. A more significant wake region indicates a more intense momentum exchange; droplets lose their transverse momentum and SMD peaks in the spray core.

The SMD curve of v_j = 12.8 m/s first increases with y/d and then decreases before the final increase, as shown in Fig. 3a. Smaller droplets were observed near the bottom wall. These droplets are generated by surface breakup and are stripped away from the periphery of the column by aerodynamic forces.[1] As Lefebvre[25] pointed out, the nonuniformity of droplet size is not necessarily disadvantageous. In some applications, the ignition source is placed near the bottom wall. Smaller droplets in the lower portion of the spray plume are beneficial for fast ignition, while larger droplets in the upper portion can provide better penetration into the airstream.

Figure 6 shows the variation of volume flux u_p and SMD for a waterjet injected at v_j = 19.3 m/s into a Mach 0.3 air crossflow at various axial locations. The curves at x/d = 300 are duplicates of those shown in Fig. 5. As x/d increases, u_p increases and approaches u_∞. A wake region can be identified at x/d = 200, although this wake region is not significant at x/d = 300 and cannot be identified at x/d = 500.

The height of the maximum flux location y_m gradually increases with axial distance, while the maximum volume flux decreases because of the increase in the spray cross-sectional area. SMD increases from about 40 to 105 μm with smaller droplets near the bottom wall. At x/d = 500, however, the SMD near the bottom wall is about 60 μm. The SMD near the bottom wall is generally larger than that found by Inamura and Nagai,[21] perhaps because of the larger airflow boundary-layer thickness in the present wind tunnel.

Inamura and Nagai[21] indicate that y_m remains constant for 1-mm jets and decreases for 2-mm jets as the axial distance increases. The discrepancy between these observations and the present results is attributed to the more intense momentum exchange between column waves and the airstream and a more

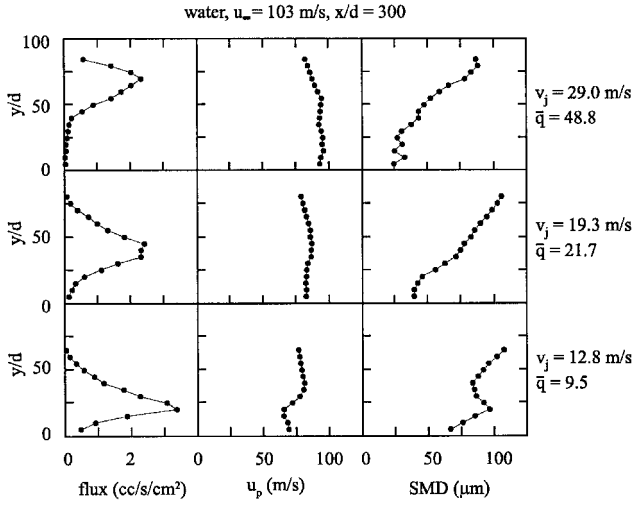

Fig. 5 Centerline properties at x/d = 300 for a waterjet injected into a Mach 0.3 airflow at various injection velocities.

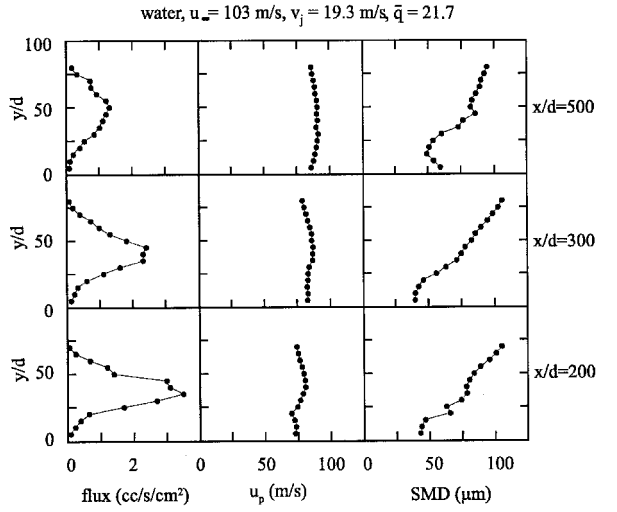

Fig. 6 Centerline properties at various axial locations of a waterjet injected into a Mach 0.3 airflow.

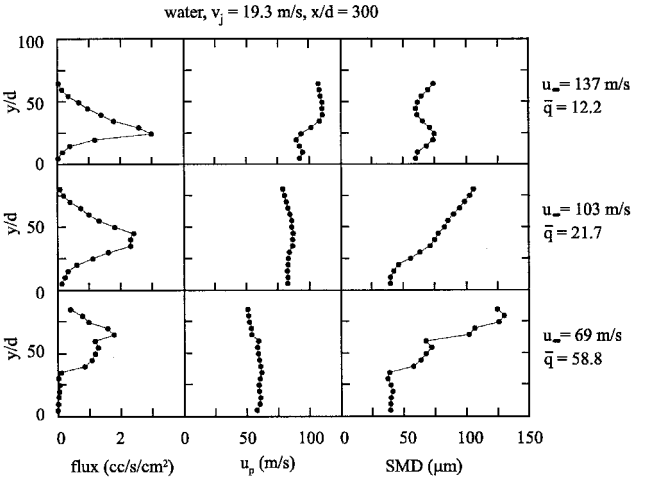

Fig. 7 Centerline properties at x/d = 300 for a waterjet injected into airflows of various Mach numbers.

significant wake region behind the column for conditions of larger d, larger u_∞, and smaller $\bar{q}$. The wake region results in a smaller flow acceleration and a larger flow residence time for droplets. Thus, gravity effects cause the spray core to move downward and cannot be neglected.

The variation of centerline properties with respect to air velocity is shown in Fig. 7. Measurements were conducted at x/d = 300. The injection velocity v_j was 19.3 m/s so that $\bar{q}$ = 12.2, 21.7, and 58.8 for u_∞ = 137, 103, and 69 m/s, respectively. The curves at u_∞ = 103 m/s were duplicated for comparison purposes. The height to the maximum volume flux location decreases as u_∞ increases because of the sharper curving of the liquid column for smaller $\bar{q}$ conditions. A wake region can be seen in the case of u_∞ = 137 m/s. Based on the present measurements it was determined that the wake region may persist for a fairly long distance and that this distance increases as u_∞ increases and as v_j decreases. This phenomenon may be attributed to the sharp curvature of the liquid column for smaller $\bar{q}$ conditions. The SMD shows trends similar to those in Figs. 5 and 6. The maximum SMD decreases as u_∞ increases, which is consistent with the observations of Wu et al.[2]

Flux-Averaged Properties

An average of SMD and u_p were calculated, weighted by the measured volume flux across the entire spray plume to provide a global droplet size, $\overline{\text{SMD}}$, and velocity $\bar{u}_p$, for each test condition. Figure 8 shows $\overline{\text{SMD}}$ and $\bar{u}_p$ vs u_∞. $\overline{\text{SMD}}$ was

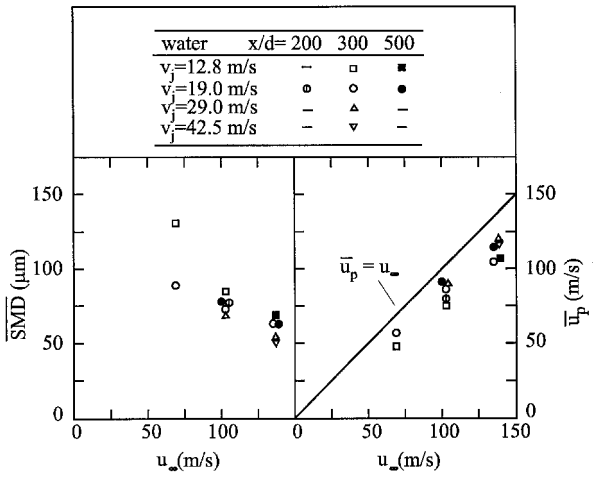

Fig. 8 Flux-averaged $\overline{SMD}$ and $\bar{u}_p$.

found to be fairly constant at the various axial locations for v_j = 19.0 m/s and u_∞ = 103 m/s, which indicates that the atomization process is complete before x/d = 200. $\overline{SMD}$ was found to decrease as u_∞ increases. Schetz and Padhye,[13] Ingebo,[10] and Nejad and Schetz[11] also observed the same trend, although Kihm et al.[20] observed an increase in $\overline{SMD}$. Furthermore, as v_j increases, $\overline{SMD}$ decreases significantly for u_∞ = 69 m/s, but only slightly for u_∞ = 103 and 137 m/s. The reduction may be explained by considering the generation of a larger number of smaller droplets because of the surface breakup for cases with larger $\bar{q}$ and We_{gd}.[1] Schetz and Padhye,[13] however, concluded that the liquid mass flow rate did not greatly affect droplet size for Mach 0.45 and 0.75 crossflows. The size correlation of Ingebo[10] does not include any dependency on injection velocity for normal injection conditions. On the other hand, Kihm et al.[20] propose that SMD is a function of $v_j^{-1.81}$. The discrepancies among these studies indicate that the variation in breakup mechanisms as v_j increases may be different for smaller u_∞ conditions as compared to larger u_∞ conditions. Further studies are required to resolve these issues. As u_∞, v_j, and x/d increase, $\bar{u}_p$ increases as shown in Fig. 8. The solid line in Fig. 8 indicates the position at which $\bar{u}_p = u_\infty$. In the present study, $\bar{u}_p$ is between 70 and 88% of u_∞.

Spray Correlations

To characterize and predict spray structures, correlations were developed for spray penetration, height of maximum flux location, width, spray cross-sectional area, and areas containing various percentages of injected liquid. Figure 9 shows the cross-sectional area of the spray plume A normalized by the injector exit area A_j. The cross-sectional area increases with $\bar{q}$ and x/d and can be correlated as

$$A/A_j = 121\bar{q}^{0.34}(x/d)^{0.52} \quad (1)$$

The mean and standard deviation of the ratio of the predicted to measured A are 1.00 and 8%, respectively. When the liquid-injection flow rate is constant, $\bar{q}$ varies with $d^{-0.2}$ by definition, and A varies with $d^{-0.6}$ according to Eq. (1). Therefore, a smaller d with a larger v_j contributes to a larger cross-sectional area. On the other hand, if the injector diameter and airflow conditions are kept the same, increases in v_j result in an increase in overall liquid concentration, because the increase in the liquid-injection flow rate is at a faster rate than the increase in cross-sectional area. Effects of these variations on fuel/air mixing and combustion efficiency, however, are not clear. Seay et al.[19] and Fuller et al.[26] suggest that the cross-sectional area could be an indicator of the degree of fuel/air mixing. However, further studies are needed to relate the mixing and combustion processes to the complex column breakup mechanisms and droplet dynamics of liquid injection in crossflows.

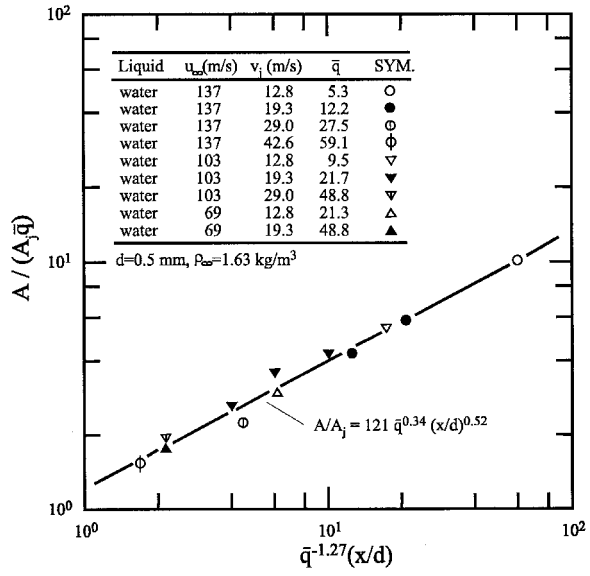

Fig. 9 Correlation and measurements of spray cross-sectional area.

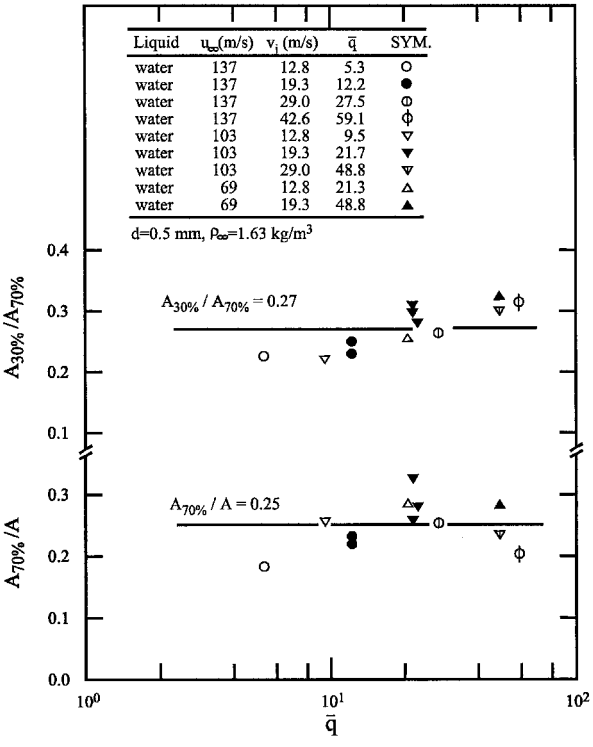

Fig. 10 Ratios of cross-sectional areas that contain various percentages of injected liquid mass.

To characterize the distribution of spray mass within the plume, areas containing 30 and 70% of the injected liquid flow rate, $A_{30\%}$ and $A_{70\%}$, are plotted in Fig. 10 as a function of $\bar{q}$. As stated previously, the measured volume flux and flux-related properties are only used to establish trends and order-of-magnitude comparisons. The ratio of $A_{70\%}/A$ yields a mean value of 0.25 with a standard deviation of 16%, whereas $A_{30\%}/A_{70\%}$ shows a mean value of 0.27 with a standard deviation of 14%. The scatter in these ratios is fairly large; nevertheless, they can provide valuable insights into the spray mass distribution within the spray plume. Thomas and Schetz[27] used a sampling probe to measure the mass distribution of a water-spray plume in a Mach 3 airflow. They found that two-thirds of the measured mass at x/d = 30 occupied only one-third of

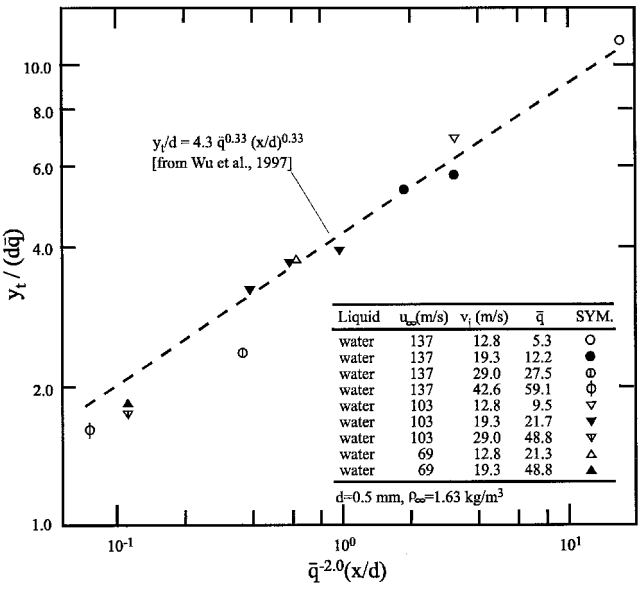

Fig. 11 Comparison of prediction and measurements of spray penetration.

the plume area. Although their experiments were conducted in supersonic flows, their observations are consistent with the present results. The ratio of $A_{30\%}/A_{70\%}$ shows a weak dependency on $\bar{q}$, although further studies are required to confirm this dependency. The measurements suggest that 70% of the injected liquid is concentrated in an area of 25% of the spray plume cross-sectional area, while 30% of the injected liquid is in an area of approximately 7% of the spray plume area. The liquid-fuel distribution within the spray plume is not uniform, therefore the determination of y_m, to be discussed later, is very important to the characterization of the location of highest droplet density.

The spray penetration y_t, defined as the largest transverse distance attained by a given spray plume, was measured and is plotted in Fig. 11. In this study, y_t was defined as the distance to the highest point along the centerline of the spray plume. Wu et al.[2] developed a correlation as

$$y_t/d = 4.3\bar{q}^{0.33}(x/d)^{0.33} \tag{2}$$

The prediction of Eq. (2) is shown as the dashed line in Fig. 11. For presentation purposes, measurements were plotted in terms of the modified variables obtained from the linear regression analysis on $\bar{q}$ and x/d. This approach is also employed for other parameters to be discussed. The current measurements were found to be generally consistent with the prediction of Eq. (2). Spray penetration increased with $\bar{q}$ and x/d. The exponent of $\bar{q}$ in Eq. (2) agrees with the 0.36 obtained by Inamura et al.[5,6] Equation (2), however, predicts a larger penetration than that observed by Inamura et al.[5,6] The discrepancy is attributed to the fact that in the present study, spray penetrations were defined as a boundary of constant volume flux measured by PDPA, while Inamura et al.[5,6] used a photographic method to locate the spray penetration. Measurements were observed to be smaller than the prediction for larger $\bar{q}$ conditions, as shown in Fig. 11. Because the PDPA receiver was installed at an angle of 30 deg above the horizontal plane, the optical path between locations near the tunnel top wall and the PDPA was blocked by the test section hardware; this blockage resulted in a smaller y_t than the actual value. Equation (2) will be used for the calculation of spray penetrations.

The height of the maximum flux location y_m was measured and shown in Fig. 12. y_m/d was found to increase with $\bar{q}$ and x/d. A correlation was obtained based on a linear regression analysis of the measurements

$$y_m/d = 0.51\bar{q}^{0.63}(x/d)^{0.41} \tag{3}$$

The mean and standard deviation of the ratio of the predicted to measured y_m are 1.00 and 12%, respectively. Equation (3), however, was developed based on results of 0.5-mm waterjets and should not be applied to liquid jets of larger diameters because of the differences in spray dynamics discussed earlier. The fit is satisfactory and indicates that y_m increases at a faster rate than y_t when $\bar{q}$ increases. This can be attributed to the sharp curving of the liquid column as discussed earlier. On the other hand, y_t is not sensitive to variations in the momentum exchange process. Therefore, the spray core region shifts upward at a faster rate than y_t, and droplets tend to be distributed to the upper portion of the plume for larger $\bar{q}$ conditions. If the distribution of most droplets to the appropriate location is a concern, y_m, in addition to y_t, is an important parameter to be considered.

Spray widths z_w were studied by measuring the maximum distance across the spray plume in the spanwise direction at

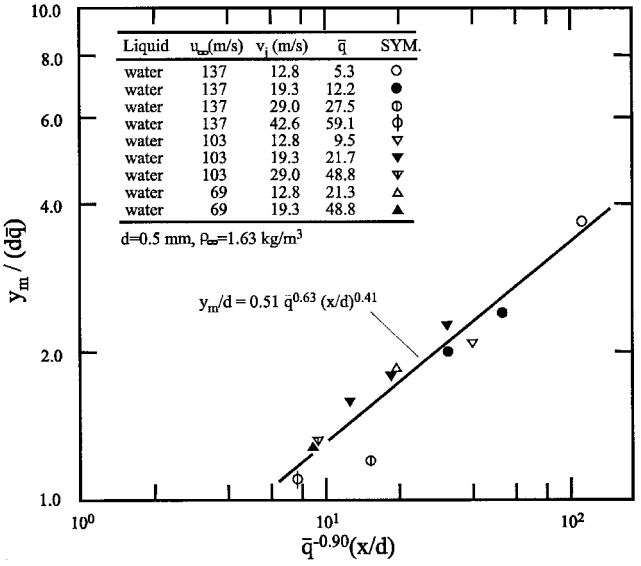

Fig. 12 Correlation and measurements of height of maximum local mass flux location.

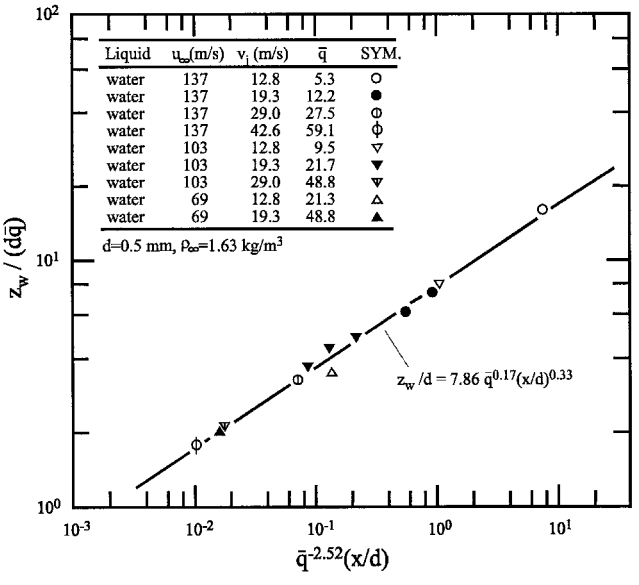

Fig. 13 Correlation and measurements of spray width.

the height of y_m. Measured z_w along with the correlation are plotted in Fig. 13. A correlation was obtained using a linear regression analysis and can be written as

$$z_w/d = 7.86\bar{q}^{0.17}(x/d)^{0.33} \quad (4)$$

The mean and standard deviation of the ratio of the predicted to measured z_w are 1.00 and 6%, respectively. The dependence of z_w/d on $\bar{q}$ is consistent with the 0.17 obtained by Oda et al.[17] and the 0.18 of Inamura et al.[5,6] As $\bar{q}$ and x/d increase, z_w increases, although the increase in z_w with $\bar{q}$ is not as significant as the increase in y_t with $\bar{q}$. Therefore, the spray plume exhibits a larger aspect ratio y_t/z_w as $\bar{q}$ increases. The ratio of y_t/z_w increases according to $d^{0.32}$ when d increases and the liquid injection flow rate is constant. According to Eqs. (2) and (4), this aspect ratio remains constant for the range of x/d tested in the present study.

Summary and Conclusions

Spray structures were measured and discussed in the present study in an effort to characterize the spray dynamics and provide a database for the development of spray control technology. Droplet sizes, axial velocities, and volume fluxes were measured using PDPA; spray structures were discussed in terms of cross-sectional distributions, centerline properties, flux-averaged properties, and spray correlations. The major conclusions of this study may be summarized as follows:

1) The distribution of droplet size in the plume exhibits a concave-layered structure with the peak on the centerline and large droplets at the top for large $\bar{q}$ conditions (Fig. 3a). Droplet sizes, however, are sometimes larger in the central portion of the spray plume when $\bar{q}$ is small (Fig. 2a). The latter observation is attributed to the sharp curving of liquid columns toward the downstream direction, which causes an intense momentum exchange between column waves and the airstream. A significant wake region can always be identified in these cases because of the intense momentum exchange.

2) Flux-averaged droplet sizes were found to be fairly constant for the x/d measured, indicating that the atomization process is complete for the present test conditions. Flux-averaged droplet size decreases as air velocity increases. For the Mach 0.3 and 0.4 cases, flux-averaged droplet size decreases as the injection velocity increases, but the decrease is not significant.

3) The cross-sectional area A increases as injection velocity and injector diameter increase, and as air freestream velocity decreases. The cross-sectional areas containing 30 and 70% of the injected liquid were also measured. Results indicate that the spray is highly concentrated in a small area and that the mass distribution within the plume is not uniform. This conclusion emphasizes the importance of the y_m/d prediction in cases requiring the distribution of most droplets to a particular location.

4) Liquid jets with a larger $\bar{q}$ tend to distribute most droplets toward the upper portion of the spray plume. A correlation of y_m was developed for a 0.5-mm waterjet, indicating that y_m increases with $\bar{q}$ and x/d. Inamura and Nagai,[21] however, observed a constant or smaller y_m as the axial distance increases for 1- and 2-mm jets. The discrepancy between these observations is attributed to the more significant momentum exchange between the liquid column and the airstream and the larger velocity deficit in the wake region behind the column for larger d, larger u_∞, and smaller $\bar{q}$ conditions.

5) Spray width z_w increases with $\bar{q}$ and x/d. The spray width, however, does not depend as strongly as y_t on $\bar{q}$, which indicates that increases in $\bar{q}$ can increase penetration more effectively than spray width. Therefore, the spray aspect ratio y_t/z_w increases with $\bar{q}$.

This study characterizes the structure of sprays from liquid-fuel jets injected into a subsonic air crossflow. Approaches to the distribution of the liquid fuel to desirable locations are suggested. However, the study was limited to water and further investigations are required to verify the effects of liquid properties on the spray structure. Effects of the air boundary-layer thickness, air turbulence structure, and injector passage design must also be investigated in the future.

Acknowledgments

This work was sponsored by and performed at the U.S. Air Force Research Laboratory, Wright–Patterson AFB, Ohio, under Contracts F33615-96-C-2614 and F33615-95-C-2566. Assistance from the Air Facility group of Research Laboratory is acknowledged. The authors would also like to thank M. R. Gruber and M. Shahnam for helpful discussion, and A. E. S. Creese for editorial comments concerning this paper.

References

[1]Wu, P.-K., Kirkendall, K. A., Fuller, R. P., and Nejad, A. S., "Breakup Processes of Liquid Jets in Subsonic Crossflows," *Journal of Propulsion and Power*, Vol. 13, No. 1, 1997, pp. 64–73.

[2]Wu, P.-K., Kirkendall, K. A., Fuller, R. P., Gruber, M. R., and Nejad, A. S., "Spray Trajectories of Liquid Fuel Jets in Subsonic Crossflows," 7th International Conf. on Liquid Atomization and Spray Systems (Seoul, Republic of Korea), Inst. of Liquid Atomization and Spray Systems, Aug. 1997.

[3]Oda, T., and Hiroyasu, H., "Breakup Model of Liquid Jet Across a High-Speed Air Stream," *Proceedings of the 9th Annual Conference on Liquid Atomization and Spray Systems* (San Francisco, CA), Inst. of Liquid Atomization and Spray Systems, 1996, pp. 99–103.

[4]Oda, T., Nishida, K., and Hiroyasu, H., "Characterization of Liquid Jet Atomization Across a High-Speed Airstream by Laser Sheet Tomography," *6th International Conference on Liquid Atomization and Spray Systems* (Rouen, France), Inst. of Liquid Atomization and Spray Systems, 1994, pp. 624–631.

[5]Inamura, T., Nagai, N., Hirai, T., and Asano, H., "Disintegration Phenomena of Metalized Slurry Fuel Jets in High Speed Air Stream," *Proceedings of the 5th International Conference on Liquid Atomization and Spray Systems* (Gaithersburg, MD), Inst. of Liquid Atomization and Spray Systems, 1991, pp. 839–846.

[6]Inamura, T., Nagai, N., Watanabe, T., and Yatsuyanagi, N., "Disintegration of Liquid and Slurry Jets Traversing Subsonic Airstreams," *Proceedings of the 3rd World Conference on Experimental Heat Transfer, Fluid Mechanics and Thermodynamics* (Honolulu, HI), Elsevier, New York, 1993, pp. 1522–1529.

[7]Nguyen, T. T., and Karagozian, A. R. "Liquid Fuel Jet in Subsonic Crossflow," *Journal of Propulsion and Power*, Vol. 8, No. 1, 1992, pp. 21–29.

[8]Fuller, R. P., Wu, P.-K., Kirkendall, K. A., and Nejad, A. S., "Effects of Injection Angle on Column Breakup Processes of Liquid Fuel Jets in Subsonic Crossflows," AIAA Paper 97-2966, July 1997.

[9]Schetz, J. A., Kush, E. A., and Joshi, P. B., "Wave Phenomena in Liquid Jet Breakup in a Supersonic Crossflow," *AIAA Journal*, Vol. 18, No. 7, 1980, pp. 774–778.

[10]Ingebo, R. D., "Aerodynamic Effects of Combustor Inlet-Air Pressure on Fuel Jet Atomization," AIAA Paper 84-1320, June 1984.

[11]Nejad, A. S., and Schetz, J. A., "Effects of Properties and Locations in the Plume on Droplet Diameter for Injection in a Supersonic Stream," *AIAA Journal*, Vol. 21, No. 7, 1983, pp. 956–961.

[12]Nejad, A. S., and Schetz, J. A., "Effects of Viscosity and Surface Tension on a Jet Plume in Supersonic Crossflow," *AIAA Journal*, Vol. 22, No. 4, 1984, pp. 653–659.

[13]Schetz, J. A., and Padhye, A., "Penetration and Breakup of Liquids in Subsonic Airstreams," *AIAA Journal*, Vol. 15, No. 10, 1977, pp. 1385–1390.

[14]Chen, T. H., Smith, C. R., Schommer, D. G., and Nejad, A. S., "Multi-Zone Behavior of Transverse Liquid Jet in High-Speed Flow," AIAA Paper 93-0453, Jan. 1993.

[15]Yates, C. L., "Liquid Injection into a Supersonic Stream," Vol. 1, Aero Propulsion Lab., AFAPL-TR-71-97, Wright–Patterson AFB, OH, 1972.

[16]Ingebo, R. D., "Penetration of Drops into High-Velocity Airstreams," NASA TM X-1363, 1967.

[17]Oda, T., Hiroyasu, H., Arai, M., and Nishida, K., "Characterization of Liquid Jet Atomization Across a High-Speed Airstream," *JSME International Journal*, Series B, Vol. 37, No. 4, 1994, pp. 937–944.

[18]Less, D. M., and Schetz, J. A., "Transient Behavior of Liquid Jets Injected Normal to a High-Velocity Gas Stream," *AIAA Journal*, Vol. 24, No. 12, 1986, pp. 1979–1986.

[19]Seay, J., McDonell, V., and Samuelsen, G., "Atomization and Dispersion from a Radial Airblast Injector in a Subsonic Crossflow," AIAA Paper 95-3001, July 1995.

[20]Kihm, K. D., Lyn, G. M., and Son, S. Y., "Atomization of Cross-Injecting Sprays into Convective Air Stream," *Atomization and Sprays*, Vol. 5, No. 4, 1995, pp. 417–433.

[21]Inamura, T., and Nagai, N., "Spray Characteristics of Liquid Jet Traversing Subsonic Airstreams," *Journal of Propulsion and Power*, Vol. 13, No. 2, 1997, pp. 250–256.

[22]Chen, T. H., Roe, L. A., and Nejad, A. S., "Multifunction Droplet Imaging and Velocimetry System for Spray Jets," *Journal of Propulsion and Power*, Vol. 10, No. 6, 1994, pp. 798–803.

[23]Raffoul, C. N., Nejad, A. S., Gould, R. D., and Spring, A. S., "An Experimental and Numerical Study of the Isothermal Flowfield Behind a Bluff Body Flameholder," American Society of Mechanical Engineers, Paper 95-GT-102, June 1995.

[24]McDonell, V. G., and Samuelsen, G. S., "Intra- and Interlaboratory Experiments to Assess Performance of Phase Doppler Interferometry," *Recent Advances in Spray Combustion: Spray Atomization and Drop Burning Phenomena, Vol. I*, edited by K. K. Kuo, Vol. 166, Progress in Astronautics and Aeronautics, AIAA, Washington, DC, 1996, pp. 57–106.

[25]Lefebvre, A. H., *Atomization and Sprays*, Hemisphere, New York, 1989, pp. 204, 205.

[26]Fuller, R. P., Wu, P.-K., Nejad, A. S., and Schetz, J. A., "Fuel-Vortex Interactions for Enhanced Mixing in Supersonic Flow," AIAA Paper 96-2661, July 1996.

[27]Thomas, R. H., and Schetz, J. A., "Distributions Across the Plume of Transverse Liquid and Slurry Jets in Supersonic Airflow," *AIAA Journal*, Vol. 23, No. 12, 1985, pp. 1892–1901.